A Series of Transition Metal Bis(dicyanobenzenedithiolate) Complexes [M(dcbdt)$_2$] (M = Fe, Co, Ni, Pd, Pt, Cu, Au and Zn)

Helena Alves,[a] Dulce Simão,[b] Isabel Cordeiro Santos,[a] Vasco Gama,[a] Rui Teives Henriques,[a,b] Horácio Novais,[b] and Manuel Almeida*[a]

Keywords: Coordination chemistry / EPR spectroscopy / Magnetic properties / S ligands / Transition metals

A series of new M[(dcbdt)$_2$]$^{-z}$ complexes of the dicyanobenzodithiolate (dcbdt) ligand with a range of transition metals (M = Co, Pd, Pt, Cu, Au and Zn) in different oxidation states (z = 0.4, 1, 2) were prepared as their nBu$_4$N salts and characterised by X-ray diffraction, cyclic voltammetry, EPR and static magnetic susceptibility. Their properties are discussed in comparison with the Ni and Fe analogues described by us recently. The structures of these complexes belong to four distinct groups: i) the Zn^{II} compound **10** is triclinic $P\bar{1}$ with the metal in a tetrahedral coordination geometry; ii) other M^{II} complexes [M = Pt (**8**), Pd (**7**), Co (**3**) and Cu (**5**)] are monoclinic $C2/m$, and are isostructural with the Ni^{II} analogue, presenting a perfectly planar square geometry; iii) the Co^{III} compound **4** is triclinic $P\bar{1}$, and isostructural with the Fe and Ni analogues, with a strong dimerisation of the M(dcbdt)$_2$ units and the metal in a square-pyramidal coordination geometry; iv) the M^{III} salts with M = Au (**2**), Cu (**6**) and Pt (**9**) are monoclinic $P2_1/c$ and the complexes are arranged as pseudo-dimers. The EPR and static magnetic-susceptibility measurements show that the Co^{II} (**3**), Cu^{II} (**5**), Pt^{III} (**9**) and Co^{III} (**4**) complexes are paramagnetic corresponding to an S = 1/2 state, except for Co^{III}, which is in a high-spin S = 1 configuration. The solid state EPR spectra of the Co^{II} compound presents a hyperfine structure typical of the I = 7/2 ^{59}Co. The temperature dependence of the paramagnetic susceptibility of the Pt^{III} compound follows a singlet-triplet model with a dimer antiferromagnetic coupling, J, of 984 K.

Introduction

During the last few years there has been a renewed interest in the study of transition metal bis(dithiolene) complexes which, in their square-planar coordination geometry, can be used as building blocks for conducting and or magnetic molecular materials.[1] These complexes can be seen as the inorganic analogues of TTF-type donors, which so far have provided the largest number of known organic conductors and superconductors, where the central C=C bond is replaced by a transition metal. In fact these inorganic complexes have frontier orbitals that are isolobal with the corresponding TTF analogues. Depending on the metal and on the oxidation state, these complexes can present different magnetic moments. Furthermore, the choice of the transition metal provides access to a diversity of different ground states. These are important features for the study and design of molecular materials with specific magnetic properties.

[a] Instituto Tecnológico e Nuclear,
Estrada Nacional no. 10, 2686-953 Sacavém, Portugal
Fax: (internat.) + 351-21-994-1455
E-mail: malmeida@itn.mces.pt
[b] Instituto Superior Técnico
Av. Rovisco Pais, 1049-001 Lisboa, Portugal
Fax: (internat.) + 351-21-841-7862
E-mail: dulce@mail.ist.utl.pt

Bis(dithiolene) complexes based on extended and delocalised π-ligands are expected to be more promising for conducting materials due to the accessibility of a wider range of oxidation states and the possibility of larger solid-state interactions.[1−4] Although bis(dithiolene) complexes of metals from groups 10 and 11 tend to adopt a square-planar geometry, favourable for extended π-π interactions and electron delocalisation in stacked structures, in some cases, namely for Fe and Co, other structures and different metal coordination environments are possible. All known Fe^{III} bis(dithiolene) complexes are dimeric with a square-pyramidal coordination geometry.[5,6] For Co^{III}, further to this dimeric structure, examples of trimeric[7] or even polymeric structures are also known.[8]

Recently, after the synthesis of the new extended aromatic ligand 4,5-dicyanobenzene-1,2-dithiolate (dcbdt), we have reported a study of the nickel complexes [Ni(dcbdt)$_2$]$^{z-}$, which can exist in a variety of different, easily accessible oxidation states (z = 0.4, 1, 2).[9] The Ni^{III} complex with this ligand and z = 1 was found to present a strongly dimerised geometry, rare for Ni, and the salt (nBu$_4$N)$_2$[Ni(dcbdt)$_2$]$_5$, with segregated stacks of partially oxidised Ni complexes, is a semiconductor with relatively high electrical conductivity. As judged from preliminary data published on the gold analogue (nBu$_4$N)$_2$-[Au(dcbdt)$_2$]$_5$,[10,11] the partially oxidised state, [M(dcbdt)$_2$]^z

  DOI: 10.1002/ejic.200300476

with $z = 0.4$, seems to be a general feature of complexes with this ligand.

More recently the iron complex $[Fe(dcbdt)_2]_2^{2-}$ was also described and it presents a similar dimerised structure, with magnetic properties similar to the Ni analogue.[12] Thus, both for fundamental reasons and also in order to evaluate their possible use as building blocks for conducting or magnetic materials, it appears of obvious interest to study similar complexes with different transition metals.

In this paper we report a comparative study of a diversity of $[M(dcbdt)_2]^z$ complexes with different transition metals: M = Fe, Co, Ni, Cu, Zn, Pd, Pt and Au.

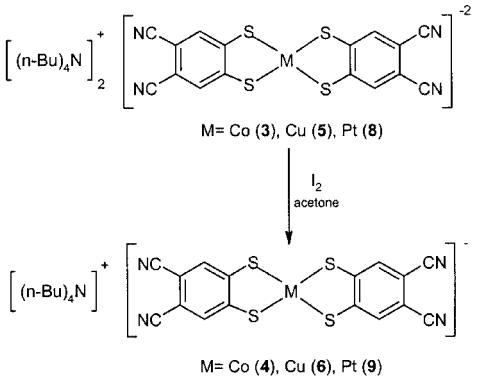

Scheme 2

Results and Discussion

Synthesis

The synthesis of the different metal complexes was performed following a general common procedure, similar to that previously described for nickel[9] and using the ligand 4,5-dicyanobenzene-1,2-dithiol (**1**) obtained from the aromatic dibenzyl sulfide 1,2-bis(benzylthio)benzene-4,5-dicarbonitrile. The benzothiol **1** was reacted, in a basic medium, with chloride salts of the different metals and the resulting metal complex precipitated as a tetrabutylammonium salt by addition of $(n\text{Bu})_4\text{Br}$ (Scheme 1).

The oxidation state of the resulting complex depends on the starting metal salt, the reaction conditions and the redox stability of the final product. The dianionic complexes were obtained from MCl_2 salts, with final yields in the range of 25−65% after recrystallisation from acetone, as deep-blue crystals for cobalt(II) (**3**), as orange crystals for palladium(II) (**7**) as red crystals for platinum(II) (**8**), as brown crystals for copper(II) (**5**) and as orange crystals for zinc(II) (**10**).

With exception of Pd and Zn, the monoanionic complexes could be obtained by oxidation of the corresponding dianions with iodine in acetone solution, as summarised in Scheme 2, leading to crystals of cobalt(III) (**4**), platinum(III) (**9**) and copper(III) (**6**) complexes, all of which are different shades of green. Attempts to oxidise the palladium(II) complex with iodine, or other oxidising agents, always led to decomposition.

The monoanionic complexes could be obtained directly after complexation for gold(III) (**2**), as green crystals, from the $KAuCl_4$ salt and also, as described previously, for iron(III) from $FeCl_3$.[12] For cobalt, the monoanionic complex $[Co(dcbdt)_2]^-$ (**4**) could also be obtained directly, starting from $CoCl_2$ and oxidation by prolonged exposure to air.

All complexes were characterised by elemental analysis (C, H, N, S) and by IR and UV/Visible spectroscopy. ^1H and ^{13}C NMR spectra were also recorded, giving rise to the expected peak-intensity ratios, according to the molecular structure and stoichiometry, for compounds **2**, **6**, **7**, **8** and **10**. For the paramagnetic compounds **4**, **5** and **9**, only the peaks of the tetrabutylammonium ion could be observed.

The cyclic voltammograms of $(n\text{Bu}_4\text{N})[M(dcbdt)_2]$ (M = Au, Co, Cu, Pt) and $(n\text{Bu}_4\text{N})_2[M(dcbdt)_2]$ (M = Pd, Zn) complexes were recorded in acetonitrile with reference to Ag/AgCl. The redox potentials observed are summarised in Table 1 together with those previously reported for the Ni and Fe compounds.

At lower potentials a redox process associated with the couple $[M(dcbdt)_2]^{2-}/[M(dcbdt)_2]^-$ is usually observed. This is reversible for M = Co ($E_{1/2} = -0.20$ V), Cu ($E_{1/2} = -0.07$ V) and Pd ($E_{1/2} = 0.36$ V), quasi-reversible for Pt ($E_{1/2} = 0.06$ V, with $\Delta E = 0.13$ V) and was not observed for Zn in the range of the experiment. An irreversible reduction wave of $[M(dcbdt)_2]^-$ to $[M(dcbdt)_2]^{2-}$ is observed for Au at −1.33 V and at −0.44 V for Fe. The difference in the oxidation potentials of the different complexes explains their chemical behaviour during the synthesis: the salts of Co, Pt, Cu, Pd, Zn are obtained in their dianionic form, $[n\text{Bu}_4\text{N}]_2[M(dcbdt)_2]$, while those of iron and gold, with

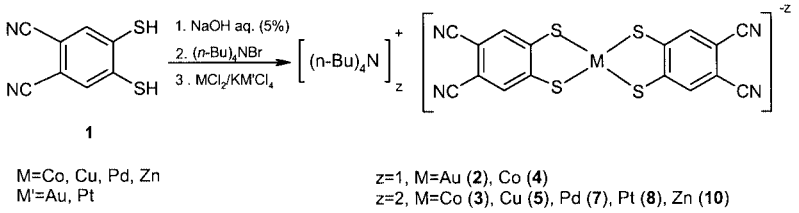

Scheme 1

Table 1. Cyclic voltammetry data of $(n\mathrm{Bu_4N})[\mathrm{M(dcbdt)_2}]$ (M = Au, Co, Cu, Pt, Fe) and $(n\mathrm{Bu_4N})_2[\mathrm{M(dcbdt)_2}]$ (M = Pd, Zn) in acetonitrile (ref. $Ag/AgNO_3$)

M	$[M(dcbdt)_2]^{2-}/[M(dcbdt)_2]^{-}$ $E_{1/2}$ [V]	$[M(dcbdt)_2]^{-}/[M(dcbdt)_2]_5^{2-}$ E_1	E_2
Pt	0.06	0.80	1.14
Pd	0.36 qr	0.80	1.02
Cu	−0.07	0.99	1.11
Co	−0.21	0.91	0.99
Au	−1.33	0.81	1.20
Fe[12]	–	0.89	1.07
Ni[9]	0.08		
Zn	–	0.89	1.27

very negative potentials for the process $[M(dcbdt)_2]^{2-}/[M(dcbdt)_2]^{-}$, are obtained in the monoanionic form $(n\mathrm{Bu_4N})[M(dcbdt)_2]$. The synthesis of the monoanionic complexes $(n\mathrm{Bu_4N})[M(dcbdt)_2]$ [M = Co (**4**), Pt (**9**) and Cu (**6**)] requires an additional oxidation step. The high redox potential for this process in the palladium complex explains the difficulty to obtain to the Pd^{III} species employing common oxidising agents. The platinum complex is also difficult to oxidise, in comparison with the other salts, which is consistent with the slightly positive potential presented. As previously found for $[Ni(dcbdt)_2]$,[9] the redox potentials of these dcbdt complexes are significantly higher than the corresponding ones in complexes with the more simple bdt (1,2-benzenedithiolate) ligand. This feature is a consequence of the electron-withdrawing nature of the CN groups, which stabilises the dianionic state. As an example, we found a potential of −0.07 V for $[Cu(dcbdt)_2]^{2-}/[Cu(dcbdt)_2]^{-}$ versus Ag/AgCl, while the corresponding potential for $Cu(bdt)_2$ is −0.56 V.[13] A similar difference in redox potentials is found for other metals.

At higher positive potentials, a series of complex oxidation processes with larger current waves occur, showing, in general, two superimposed waves, which can be associated with a multielectron transfer process leading to the formation of $[M(dcbdt)_2]_5^{2-}$ (Scheme 3), similar to previous observations for M = Ni.[9]

$$5[M(dcbdt)_2]^{-} \rightleftharpoons [M(dcbdt)_2]_5^{2-} + 3e^{-}$$

Scheme 3

In fact, the compounds $(n\mathrm{Bu_4N})_2[M(dcbdt)_2]_5^{2-}$ (M = Au and Ni) have already been obtained by electrocrystallisation,[9,10] and a study of similar compounds, with different transition metals, will be reported in a subsequent publication.[14]

X-ray Diffraction Studies

The crystals obtained for compounds **3**, **4**, **7**, **8** and **10** enabled their crystal structure determination by X-ray diffraction. The refinement of the crystal structures of compounds **2**, **6** and **9** was limited by a small degree of disorder affecting only the cation. The reduced diffraction power of the crystals of compound **5** allowed only the determination of the lattice parameters, which are similar to those of Pt, Pd and Co. Crystallographic data of these compounds are listed in Table 2 and 3.

Table 2. Crystallographic data for compounds $(n\mathrm{Bu_4N})_2[\mathrm{M(dcbdt)_2}]$ (M = Co, Pd, Pt, Zn)

	Co (**3**)	Pd (**7**)	Pt (**8**)	Zn (**10**)
Crystal size (mm)	0.8 × 0.7 × 0.6	0.6 × 0.24 × 0.16	0.8 × 0.7 × 0.4	0. 7 × 0.3 × 0.2
Crystal Colour and shape	dark-blue prism	orange plate	red prism	orange prism
Empirical formula	$C_{48}H_{76}CoN_6S_4$	$C_{48}H_{76}N_6S_4Pd$	$C_{48}H_{76}N_6S_4Pt$	$C_{48}H_{76}N_6S_4Zn$
Molecular mass	924.32	971.79	1060.48	930.76
Crystal system	monoclinic	monoclinic	monoclinic	triclinic
Space group (no.)	*C*2/*m* (12)	*C*2/*m* (12)	*C*2/*m* (12)	$P\bar{1}$ (2)
a (Å)	19.6405(20)	19.6043(8)	19.6071(9)	12.9364(20)
b (Å)	13.4112(19)	13.4907(10)	13.4674(6)	14.9367(10)
c (Å)	9.7637(14)	9.7772(8)	9.7599(4)	15.8187(17)
α (°)				70.6391(94)
β (°)	94.005(10)	93.150(5)	93.300(4)	79.7745(83)
γ (°)				80.0083(92)
V (Å^3)	2565.5(2)	2581.9(3)	2572.9(2)	2715.8(6)
Z, $D_{calcd.}$ (Mg/m^3)	2, 1.197	2, 1.250	2, 1.369	2, 1.138
μ (mm^{-1})	4.419	0.558	2.926	0.641
F(000)	994	1032	1096	1000
Theta range (°)	4.51 to 72.62	1.83 to 26.06	1.84 to 27.99	1.67 to 25.98
Index range (*h*,*k*,*l*)	−23/23, 0/16, −11/0	−24/24, −16/0, 0/−12	−25/25, −17/0, −12/0	−15/15, −18/17, −19/0
Refl. collected	2414	2785	3315	10733
Refl. unique/R_{int}	2272/R_{int} = 0.0385	2626/R_{int} = 0.0283	3141/R_{int} = 0.0118	10340/R_{int} = 0.0215
T max./min.	0.9962/0.3368	0.9998/0.9693	0.9999/0.9023	0.9995/0.9400
No. of refined parameters	155	154	154	532
Goodness-of-fit on F^2	1.044	1.084	1.084	1.016
Final R_1, [$I > 2\sigma(I)$], wR_2	0.0581/0.1389	0.0519/0.0949	0.0353/ 0.0747	0.0626/0.1278

Table 3. Crystallographic data for compounds (nBu$_4$N)[M(dcbdt)$_2$] (M = Au, Co, Cu, Pt)

	Au (**2**)	Co (**4**)	Cu (**6**)	Pt (**9**)
Crystal size [mm]	0.40 × 0.20 × 0.04	0.82 × 0.22 × 0.20	0.60 × 0.20 × 0.10	0.30 × 0.30 × 0.05
Crystal Colour/Shape	green plate	dark-green needle	dark-green needle	green plate
Empirical formula	$C_{32}H_{40}N_5S_4Au$	$C_{32}H_{40}N_5S_4Co$	$C_{32}H_{40}N_5S_4Cu$	$C_{32}H_{40}N_5S_4Pt$
Molecular mass	819.90	681.87	686.47	818.02
Crystal System	monoclinic	triclinic	monoclinic	monoclinic
Space group	$P2_1/c$	$P\bar{1}$	$P2_1/c$	$P2_1/c$
a (Å)	7.9094(6)	9.481(2)	7.8539(2)	7.9032(8)
b (Å)	20.918(3)	13.096(2)	20.9006(9)	20.837(2)
c (Å)	20.624(3)	15.917(3)	20.6126(6)	20.5885(16)
α (°)		66.642(10)		
β (°)	90.294(9)	86.285(16)	90.351(3)	90.147(7)
γ (°)		70.358(10)		
V (Å^3)	3412.0(7)	1703.7(5)	3383.5(2)	3390.5(6)
Z, $D_{calcd.}$ (Mg/m^3)	4, 1.596	1.329	4, 1.348	4, 1.603
μ (mm^{-1})	4.586	0.778	3.442	4.415
F(000)	1640	716	1440	1636
Theta range (°)	1.97 to 24.96	1.79 to 25.97	3.01 to 72.01	2.19 to 26.98
Index range (h,k,l)	−9/0, −24/0, −24/−24	−11/11, −16/15, −19/1	−1/9, −24/0, −24/24	−10/0, −26/0, −26/26
Refl. collected	6278	7389	7288	3393
Refl. unique/R_{int}	5827/R_{int} = 0.1111	6634/R_{int} = 0.0225	5914/R_{int} = 0.0396	7310/R_{int} = 0.0343
T max./min.	0.8967/0.4629	0.9990/0.8922	0.9999/0.6905	0.9991/0.4272
No of refined parameters	319	398	506	7310/16/369
Goodness-of-fit on F^2	1.000	1.037	1.036	1.033
Final R_1, [$I > 2\sigma(I)$], wR_2	0.0835/0.1776	0.0640/0.1548	0.0784/0.1965	0.0773/0.1696

The structures observed can be classified into the following four groups: *i*) the Zn^{II} compound is triclinic, $P\bar{1}$, with the metal in a tetrahedral coordination geometry; *ii*) the other M^{II} complexes (M = Pt, Pd, Co and Cu) are monoclinic, $C2/m$, and isostructural with the Ni^{II} analogue described previously,[9] presenting a perfectly square-planar geometry; *iii*) the Co^{III} compound is triclinic, $P\bar{1}$, and isostructural with the Fe[12] and Ni[9] analogues, with a strong dimerisation of the M(dcbdt)$_2$ units and the metal in a square-pyramidal coordination geometry; *iv*) the M^{III} complexes with M = Au, Cu and Pt are monoclinic, $P2_1/c$, and present the complexes as pseudo-dimers.

Among the M^{II} complexes, the crystal structures of the (nBu$_4$N)$_2$[M(dcbdt)$_2$] salts with M = Co (**3**), Pd (**7**), Pt (**8**), and Zn (**10**) were determined by X-ray diffraction and their crystallographic data are listed in Table 2. For M = Cu (**5**) only the unit-cell parameters could be obtained, monoclinic, $C2/m$, with a = 19.753 Å, b = 13.440 Å, c = 9.792 Å, β = 93.44°, indicating a structure similar to those of Pt, Pd and Co. These compounds are isostructural with (nBu$_4$N)$_2$-[Ni(dcbdt)$_2$], described previously.[9]

Figure 1 presents the ORTEP diagrams of the complex anions in compounds **3**, **4**, **6** and **10**, showing the atomic labelling scheme, which is the same in the analogous compounds **2**, **7**, **8**, **9** with different metals; selected bond lengths and angles for these compounds are presented in Table 4 and Table 5.

In compound **10**, the [Zn(dcbdt)$_2$]$^{2-}$ anion is located in a general position and the metal has a tetrahedral coordination geometry. The average Zn−S bond length (2.316 Å) is similar to those found in many other Zn^{II} bis(dithiolate) complexes.[15−17] The ligands preserve their planarity (rms atomic deviations are 0.008 and 0.011 Å) but they present a dihedral angle of 78.28°. The Zn atom is significantly deviated (0.337 Å) from the average plane of the ligand containing S1 and S2, while it is much less deviated (0.028 Å) from the average plane of the second ligand containing S3 and S4. This distortion is imposed by the crystal packing, in which the anionic complexes are well separated by the cations, as shown in Figure 2. There are several hydrogen bonds between cation and anion units but this alternating packing prevents any possible interaction between the anion units.

In compounds **3**, **7** and **8** the transition metal atom is located at an inversion centre and the [M(dcbdt)$_2$]$^{2-}$ dianion presents a perfectly planar geometry, since all atoms lie in a mirror plane. The crystal structure of these compounds is made up of [M(dcbdt)$_2$]$^{2-}$ layers containing mirror planes at y = 0 and y = 1/2. These layers are separated by cation layers, as shown in Figure 3 for M = Co, thus preventing any short anion-anion interactions.

In **4** the Co^{III} complex presents a strong dimerisation of the [Co(dcbdt)$_2$]$^-$ units that are related by an inversion centre (iv in Figure 1) located between the two cobalt atoms. In the [Co(dcbdt)$_2$]$_2^{2-}$ units, besides the equatorial Co−S bonds, with distances Co−S(1) 2.1780(13) Å, Co−S(2) 2.1902(13) Å, Co−S(3) 2.1823(12) Å and Co−S(4) 2.2000(13) Å, there are two apical Co−S(3)* bonds at 2.3638(13) Å with a Co−Co* distance of 3.1534(10) Å. This dimerisation is typical of many Co^{III} bisdithiolene complexes,[5,6,18−20] with the metal presenting a square-pyramidal coordination geometry, with a metal-over-sulfur overlap mode, equatorial Co−S distances typically in the range 2.16−2.19 Å and apical Co−S bond lengths varying

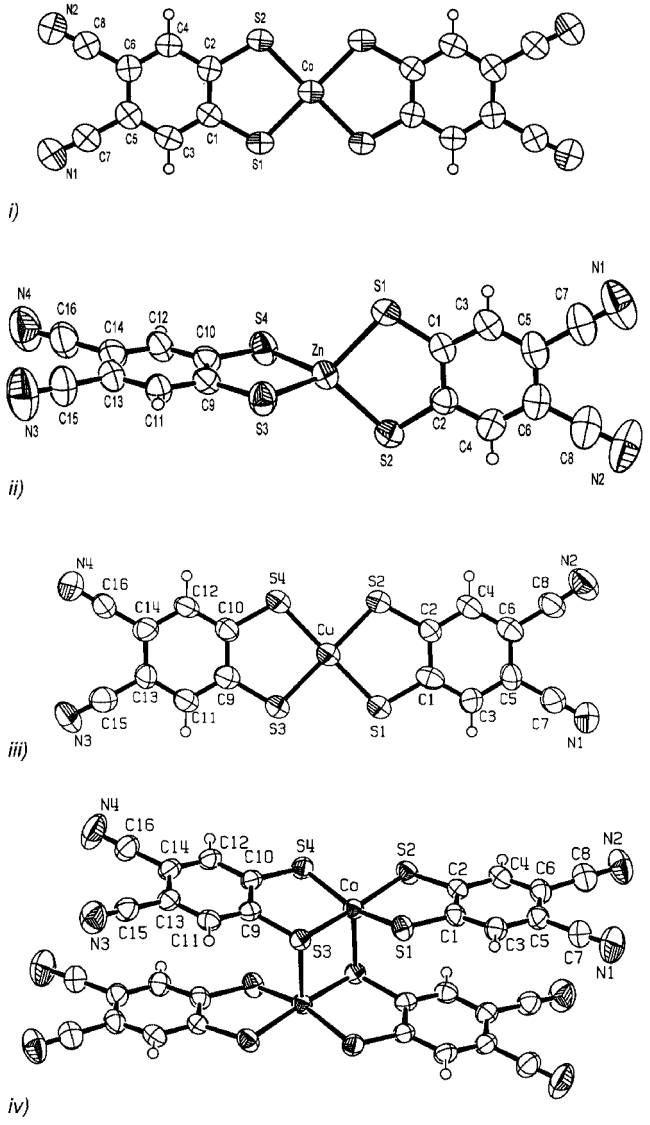

Figure 1. ORTEP diagrams: (i) $[Co(dcbdt)_2]^{2-}$ dianion in **3**, (ii) $[Zn(dcbdt)_2]^{2-}$ dianion in **10**, (iii) $[Cu(dcbdt)_2]^{-}$ monoanion in **6** and (iv) $[Co(dcbdt)_2]_2^{2-}$ in **4**; the diagrams are drawn with 50% probability thermal ellipsoids; the adopted numbering scheme is the same in isostructural compounds **2**, **7**, **8** and **9**

from 2.38 to 2.43 Å. As shown in Figure 4 (see a) the ligands are slightly distorted, repelling each other and making the distance between their mean planes larger than the central Co−S distance.

The crystal structure of **4** is identical to those of the Ni and Fe analogues previously described by us.[9,12] Along the *c* and *b* axes the dimerised anions and the cations are alternating, whereas along the *a* axis the $[Co(dcbdt)_2]_2^{2-}$ dimers are arranged in chains due to several weak interactions connecting two side-by-side $[Co(dcbdt)_2]^{-}$ units of adjacent dimers, namely the hydrogen bonds N(4)···H(4*) and N(4*)···H(4) at 2.609 Å and 156°, S(4)···H(12) at 3.248 Å and a short S(4)···S(4*) contact at 3.817 Å (see Figure 5).

In the other M^{III} complexes with M = Au (**2**), Cu (**6**) and Pt (**9**), the anions are located in a general position near the inversion centres and therefore form pseudo-dimers, as

Table 4. Selected bond lengths [Å] for $(nBu_4N)_2[M(dcbdt)_2]$ (M = Co, Pd, Pt, Zn)

	Co (**3**)	Pd (**7**)	Pt (**8**)	Zn (**10**)
M−S(1)	2.1754(11)	2.2930(13)	2.2710(10)	2.3240(11)
M−S(2)	2.1830(10)	2.2849(15)	2.2694(12)	2.3107(12)
M−S(3)				2.3273(11)
M−S(4)				2.3047(12)
S(1)−C(1)	1.746(4)	1.742(5)	1.742(4)	1.734(4)
S(2)−C(2)	1.744(4)	1.735(6)	1.732(5)	1.747(4)
S(3)−C(9)				1.747(4)
S(4)−C(10)				1.749(4)
C(1)−C(2)	1.389(6)	1.408(7)	1.403(6)	1.430(5)
C(1)−C(3)	1.400(6)	1.401(7)	1.401(6)	1.383(5)
C(4)−C(2)	1.412(5)	1.398(7)	1.405(7)	1.381(5)
C(4)−C(6)	1.381(6)	1.385(7)	1.385(7)	1.375(5)
C(5)−C(3)	1.378(6)	1.386(7)	1.388(7)	1.377(6)
C(5)−C(6)	1.413(6)	1.394(7)	1.394(7)	1.402(6)
C(5)−C(7)	1.433(6)	1.441(7)	1.438(7)	1.437(6)
C(6)−C(8)	1.440(6)	1.439(8)	1.444(7)	1.449(6)
C(7)−N(1)	1.141(6)	1.137(7)	1.142(7)	1.133(6)
C(8)−N(2)	1.137(6)	1.134(7)	1.148(6)	1.135(6)
C(9)−C(11)				1.395(5)
C(9)−C(10)				1.413(5)
C(10)−C(12)				1.372(5)
C(14)−C(12)				1.379(5)
C(11)−C(13)				1.382(5)
C(13)−C(14)				1.390(5)
C(13)−C(15)				1.419(5)
C(14)−C(16)				1.437(6)
C(15)−N(3)				1.145(5)
C(16)−N(4)				1.136(5)

shown in Figure 6 for **9**. The values of the M−S bond lengths in these complexes, presented in Table 5, are similar to the values published for other monoanionic bis(dithiolene) complexes. A remarkable common feature of these pseudo-dimers is that the complex units deviate only slightly from planarity in such a way that the ligands are closer than the central MS_4 atoms (Figure 4; see b for **6**, c for **2** and d for **9**). In fact, the distance between the average planes defined by the benzene rings of neighbouring complex units is about 3.43 Å, and almost the same for all three metal complexes, whereas the planes of the central MS_4 atoms within the dimer are further apart by 0.15 Å, 0.20 Å, and 0.23 Å for Cu, Pt, and Au, respectively (see Table 6). This is at variance with the strong Co, Fe and Ni dimers previously described, where there are two short M−S central bonds and a distortion of the ligands separating their extremities from each other (Figure 4, a).

The relatively short distance between the benzene rings clearly denotes the existence of a significant ligand−ligand interaction in the present complexes. In this respect it is worthwhile to mention that in **9** the overlap mode between the two closest $M(dcbdt)_2$ units is obtained by a small shift along the short axis of the complexes, leading to a more direct metal−metal interaction, while for **6** and **2** the overlap is obtained by shifts along both the long and short axes, leading to both metal−metal and metal−sulfur interactions.

It is also worthwhile to note that while along the *b* and *c* axes the dimers alternate with cations without any short

Table 5. Selected bond lengths (Å) for (nBu$_4$N)[M(dcbdt)$_2$] (M = Au, Co, Cu, Pt)

	Au (**2**)	Co (**4**)	Cu (**6**)	Pt (**9**)
M−S(1)	2.311(4)	2.1780(13)	2.1843(19)	2.255(3)
M−S(2)	2.298(4)	2.1902(13)	2.1743(18)	2.261(3)
M−S(3)	2.312(4)	2.1823(12)	2.1786(18)	2.267(3)
M−S(4)	2.302(4)	2.2000(13)	2.176(2)	2.269(3)
M−S(3)#1[a]		2.3638(13)		
S(1)−C(1)	1.753(13)	1.723(4)	1.755(6)	1.725(12)
S(2)−C(2)	1.760(15)	1.726(4)	1.757(6)	1.732(11)
S(3)−C(9)	1.714(19)	1.749(4)	1.739(7)	1.744(13)
S(4)−C(10)	1.765(18)	1.721(4)	1.736(6)	1.728(11)
C(1)−C(2)	1.42(2)	1.422(6)	1.409(8)	1.385(15)
C(1)−C(3)	1.38(2)	1.387(6)	1.393(9)	1.396(16)
C(2)−C(4)	1.34(2)	1.394(6)	1.368(8)	1.406(15)
C(4)−C(6)	1.38(2)	1.373(7)	1.379(9)	1.365(16)
C(5)−C(3)	1.36(2)	1.373(6)	1.378(8)	1.370(16)
C(5)−C(7)	1.43(2)	1.445(7)	1.428(9)	1.443(17)
C(6)−C(5)	1.44(2)	1.409(7)	1.404(9)	1.413(16)
C(6)−C(8)	1.41(2)	1.432(7)	1.436(8)	1.447(16)
C(7)−N(1)	1.17(2)	1.117(7)	1.128(8)	1.123(16)
C(8)−N(2)	1.15(2)	1.152(6)	1.128(8)	1.129(16)
C(10)−C(12)	1.34(2)	1.408(6)	1.381(8)	1.430(15)
C(10)−C(9)	1.45(2)	1.409(6)	1.418(8)	1.385(17)
C(11)−C(9)	1.39(2)	1.384(6)	1.403(8)	1.390(16)
C(12)−C(14)	1.41(2)	1.369(6)	1.389(8)	1.372(16)
C(13)−C(11)	1.42(2)	1.375(6)	1.394(8)	1.381(16)
C(13)−C(15)	1.45(3)	1.429(7)	1.442(9)	1.440(17)
C(14)−C(13)	1.42(2)	1.416(6)	1.395(8)	1.421(16)
C(14)−C(16)	1.43(2)	1.445(7)	1.418(9)	1.440(17)
C(15)−N(3)	1.07(2)	1.121(6)	1.159(8)	1.135(16)
C(16)−N(4)	1.17(2)	1.121(7)	1.144(9)	1.140(16)

[a] #1 $-x, -y, -z + 1$.

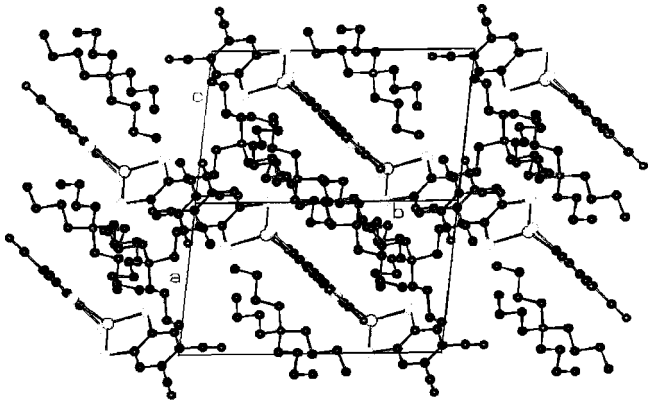

Figure 2. View of the crystal structure of (nBu$_4$N)$_2$[Zn(dcbdt)$_2$] (**10**) along the [101] direction

inter-dimer contacts in the *b*,*c* plane, along *a* they are connected in chains through short S2−S3* contacts at 3.692(4) Å and hydrogen bonds N2−H3* and N3−H12* at 2.628(11) Å and 2.554(11) Å, respectively, as shown in Figure 7 for **9**. The interplanar distances and the short inter- and intra-dimer distances observed for **2**, **4**, **6** and **9** are given in Table 6.

Magnetic Properties

The M^{II} complexes of Co (**3**) and Cu (**5**), as d^7 and d^9 species respectively, and the Pt^{III} (**9**) complex, as a d^7 system, are expected to be paramagnetic with one unpaired electron. The Ni^{III} and the Fe^{III} complexes were previously described as paramagnetic with $S = 1/2$.[9,12] The remaining complexes of this family presented in this paper are expected to be diamagnetic. These expectations were con-

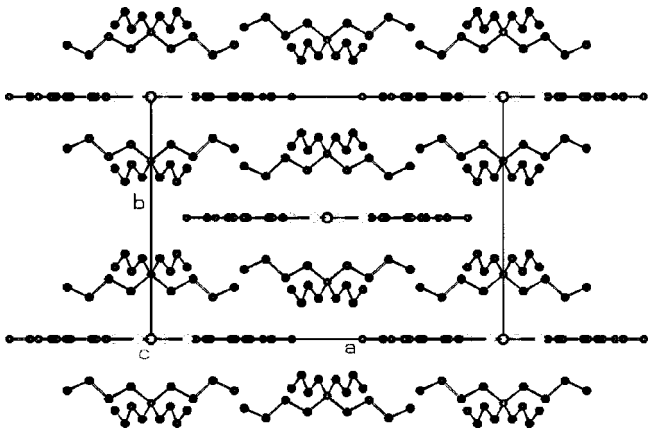

Figure 3. View of the crystal structure of (nBu$_4$N)$_2$[Co(dcbdt)$_2$] (**3**) along the *c* axis

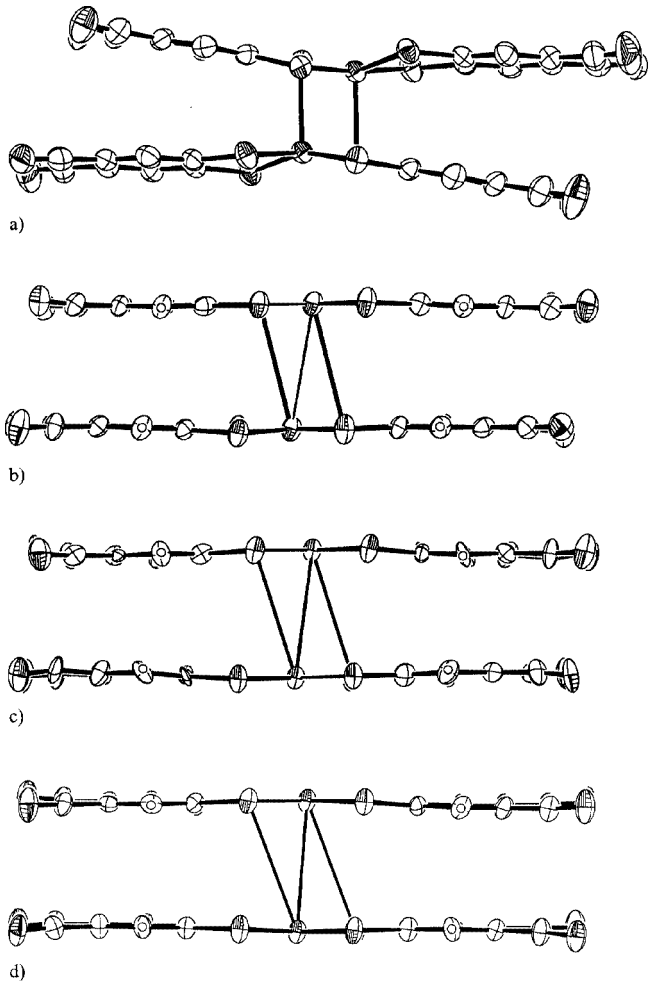

Figure 4. Side view of: a) the [Co(dcbdt)$_2$]$_2$ dimer in **4**, b) the [Cu(dcbdt)$_2$]$_2$ pseudo-dimer in **6**, c) the [Au(dcbdt)$_2$]$_2$ pseudo-dimer in **2** and d) the [Pt(dcbdt)$_2$]$_2$ pseudo-dimer in **9**

Table 6. Distances (Å) between complex units in $(n\mathrm{Bu_4N})[\mathrm{M(dcbdt)_2}]$ compounds

M	Au(**2**)	Co(**4**)	Cu(**6**)	Pt(**9**)
Interplanar:				
MS_4-MS_4	3.67		3.60	3.63
Bz−Bz	3.43		3.45	3.42
Intradimer:				
M···M*	4.057(2)[a]	3.153(1)[b]	3.960(1)[a]	3.909(1)[a]
M···S*	3.822(6)[a]	2.364(1)[b]	3.648(2)[a]	3.915(4)[a]
Interdimer:	S2−S3[c] 3.626(5)	S4−S[d] 3.8117(2)	S1−S4[c] 3.772(2)	S2−S3[c] 3.692(4)
	N2−H3[c] 2.668(16)	N4−H4[d] 2.609(6)	N1−H4[c] 2.574(7)	N2−H3[c] 2.628(11)
	N3−H12[c] 2.578(17)		N4−H11[c] 2.524(7)	N3−H12[c] 2.554(11)

[a] $-x,1-y,1-z$. [b] $-x,-y,-z+1$. [c] $x\pm1,y,z$. [d] $1-x,-y,1-z$.

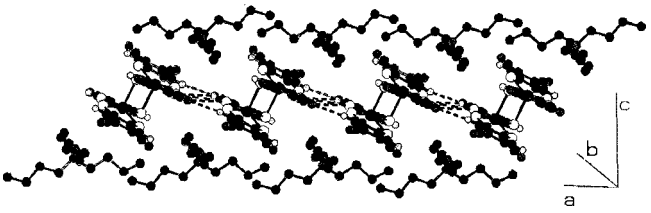

Figure 5. Crystal packing of $(n\mathrm{Bu_4N})_2[\mathrm{Co(dcbdt)_2}]_2$ (**4**), showing the side-by-side interactions between the $\mathrm{Co(dcbdt)_2}$ dimers along the *a* axis

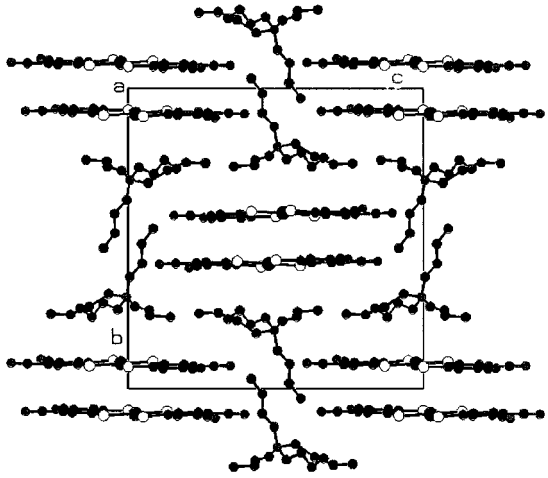

Figure 6. Crystal structure of $(n\mathrm{Bu_4N})_2[\mathrm{Pt(dcbdt)_2}]_2$ (**9**) viewed along the *a* axis

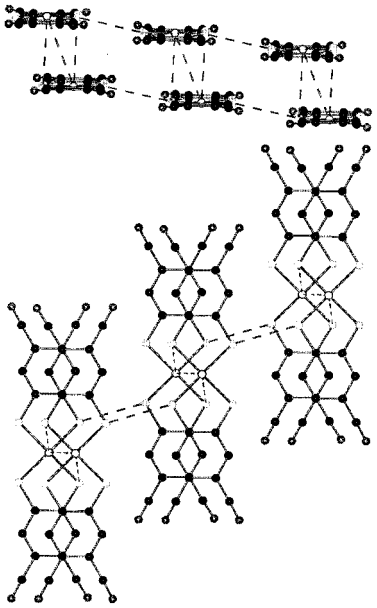

Figure 7. Side and top view of the chains, along the *a* axis, of $\mathrm{Pt(dcbdt)_2^-}$ pairs in compound **9**; the dashed lines emphasise the close interactions between the pairs and within a pair

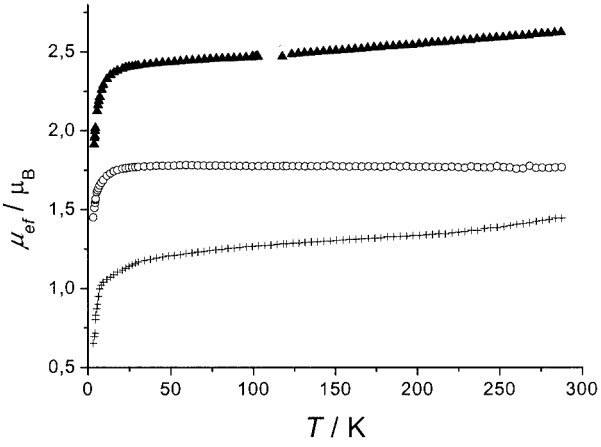

Figure 8. Effective magnetic moments as a function of temperature of $(n\mathrm{Bu_4N})_2[\mathrm{Cu(dcbdt)_2}]$ (**3**) (circles), $(n\mathrm{Bu_4N})_2[\mathrm{Co(dcbdt)_2}]$ (**4**) (triangles) and $(n\mathrm{Bu_4N})_2[\mathrm{Co(dcbdt)_2}]_2$ (**5**) (crosses)

firmed by EPR spectroscopic and static magnetic susceptibility measurements, with the exception of the $\mathrm{Co^{III}}$ complex which, as a d^6 system, seems to have a high-spin $S = 1$ configuration.

The EPR spectrum of an acetone solution of **5** at room temperature exhibits a quadruplet of lines, centred at $g = 2.045$ with an average hyperfine field constant of, a_o, of 80.8 G, due to the hyperfine interaction of the electron spin with the nuclear $I = 3/2$ spin of the copper nuclides. The powder EPR spectrum presents a pattern typical of a system with axial symmetry ($g_{\|} = 2.082$ and $g_{\perp} = 2.024$).

The static paramagnetic susceptibility, χ_P, of **5**, calculated from raw data assuming a diamagnetic contribution of -6.14×10^{-4} emu/mol, as estimated from tabulated Pascal constants, leads to an effective magnetic moment, $\mu_{eff.}$, of 1.77 μ_B. As shown in Figure 8, this value remains fairly constant above 20 K, (Figure 8) and is very close to the one

expected for an $S = 1/2$ system with $g = 2$. Below 20 K there is a reduction of μ_{eff}, denoting the presence of minor antiferromagnetic interactions.

Single crystals of $(n\mathrm{Bu_4N})_2[\mathrm{Co(dcbdt)_2}]$ (**3**) at room temperature present a complex EPR signal of an octet of lines with variable separation, depending on the crystal orientation (Figure 9). This type of spectra is typical of the hyperfine structure due to the $I = 7/2$ spin of ^{59}Co.[21−23] However this hyperfine structure is observed only for particular orientations and the signal presents a strong g-factor anisotropy.

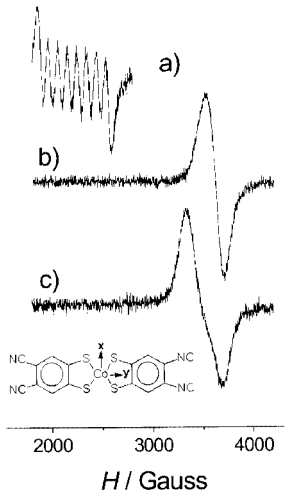

Figure 9. EPR spectra of a single crystal of $(n\mathrm{Bu_4N})_2[\mathrm{Co(dcbdt)_2}]$ (**4**) at 300 K, with the magnetic field in the b,c plane for two orientations 90° apart: a) along the long axis of the complex, b) along the short axis in the plane of the complex, c) perpendicular to the plane of the complex

A study of the EPR spectra with oriented single crystals allowed us to deduce an almost uniaxial rhombic anisotropy related to the symmetry axes of the complex as well as the anisotropy of the hyperfine tensor a_0. The principal axes of the a_0- and g-tensors are expected to coincide. As previously discussed in the crystallographic section, the Co^{II} complex is planar and lies parallel to the a,c plane, with the long axis making an angle of approximately 29° with a. The narrowest signal, with an apparent single EPR line with a peak-to-peak width of 14.6 mT, and the minimum g value at $g_x = 1.936$ is observed when the magnetic field is along the short axis in the plane of the complex (Figure 9, a). Along this direction the hyperfine coupling constant is negligible ($A_x < 2$ mT).

When the magnetic field is along the long axis in the plane of the complex, the maximum width is observed in the EPR signal that presents an octet extending over 73.4 mT and centred at $g_y = 3.156$ (Figure 9, a). Deviations of ±40° from this g_{max} orientation still present an octet with negligible extent variations of only ±1 mT. An octet is observed over all this angular range, corresponding to a hyperfine coupling constant, A_y, of 9.2 mT.

An intermediate situation is observed when the magnetic field is perpendicular to the plane of the complex (along the b axis). For this orientation an EPR signal with no resolved octet but well-separated maxima and minima, corresponding to a linewidth of 35.7 mT, is observed centred at $g_z = 1.994$. This suggests a small hyperfine component for this direction of $A_z = 4.5$ mT.

To the best of our knowledge this is the first example of a pure Co compound in which hyperfine structure is observed in the solid state. The hyperfine structure can be observed without the interference of significant dipolar interactions thanks to the large separation of the complexes in the structure, where the closest Co−Co distance is 9.76 Å along c, without any contact between the anions, and 12.4 Å between different layers separated by the cations. A detailed analysis of the observed anisotropy in the A and g-tensors in terms of the metal and ligand orbitals involved in the SOMO will be the subject of a subsequent publication.

The static paramagnetic susceptibility of **3** leads, in a similar way, to an effective magnetic moment, μ_{eff}, significantly larger than that of the Cu analogue (Figure 8). At room temperature μ_{eff} is about 2.55 μ_B, which decreases almost linearly with temperature upon cooling to 2.40 μ_B at 20 K. Below this temperature a more drastic reduction of μ_{eff} is observed. This larger magnetic moment is in fair agreement with the larger average g-value observed in the EPR spectrum, since for $g = 2.82$ and $S = 1/2$ a μ_{eff} value of 2.44 μ_B is expected. The small linear decrease of the effective moment observed between room temperature and 20 K most probably denotes the presence of a non-negligible temperature-independent paramagnetism.

Compound **9** is EPR silent at room temperature, as is also the case for the Ni and Fe analogues. Below 110 K a signal starts to appear, as shown in Figure 10 for a powder at 60 K. This signal can be described as coming from a doublet $S = 1/2$ state showing rhombic anisotropy with $g_x = 2.246$, $g_y = 2.054$ and $g_z = 1.785$. The more intense lines correspond to $I = 0$ platinum isotopes (66.2% natural

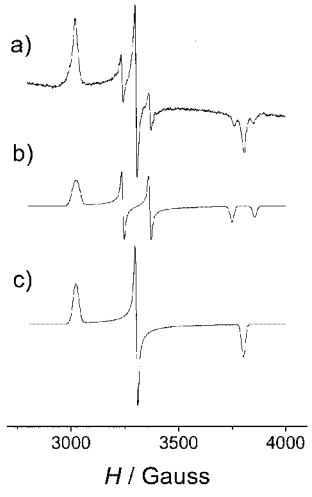

Figure 10. Experimental EPR spectra of $(n\mathrm{Bu_4N})[\mathrm{Pt(dcbdt)_2}]$ (**9**) as a polycrystalline sample at 60 K: (a) simulated spectra for 33.8% natural abundance of ^{195}Pt isotope with $I = 1/2$, and $A_x = 0$ mT, $A_y = 13$ mT and $A_z = 9.3$ mT (b), and 66.2% of Pt isotopes with $I = 0$ (c), both with $g_x = 2.246$, $g_y = 2.054$, $g_z = 1.785$

abundance), and the satellites around the medium- and high-field components are due to the 33.8% natural abundance of the ^{195}Pt isotope with $I = 1/2$. The anisotropic hyperfine coupling tensor has $A_x < 4$ mT (the satellites are not resolved for this component), $A_y = 13$ mT and $A_z = 9.3$ mT. Assuming a situation similar to $Pt(mnt)_2^-$, and the same coordinate system,[24] x is the shortest axis in the plane of the complex, y the longest and z is normal to the plane of the complex.

As, in this compound, the magnetic susceptibility follows a single-triplet model due to the dimerisation of $[Pt(dcbdt)_2]^-$, we looked for a possible signature of the $S = 1$ state in the EPR spectrum. The half-field signal corresponding to the forbidden $\Delta M_S = 2$ transition, was only visible at 4.2 K as a weak signal. Other signals coming from the triplet $S = 1$ state, if existing, are obscured by the spectrum of the doublet state described above.

The observation of an EPR signal of the triplet state in metal complexes is, in general rare, and most dimerised complexes are EPR silent, as reported for $(n\mathrm{Bu_4N})[Ni(dcbdt)_2]$[9] and $(n\mathrm{Bu_4N})[Fe(dcbdt)_2]$;[12] the number of Pt^{III} complexes studied by EPR spectroscopy is small. The $[Pt(dmit)_2]^-$ species, which is isolated and undimerised, presents a smaller g anisotropy than the present compound, with a hyperfine coupling being detected.[25] $[Pt(mnt)_2]^-$, also an undimerised species, studied by Kirmse et al. as a diluted paramagnetic centre in a diamagnetic host, shows a large anisotropy of the hyperfine coupling tensor, with $A_x = 0$.[24] In the *cis*-diammineplatinum α-pyridone complex, a mixed-valence compound, there is dimer formation, with the Pt−Pt distance of 2.7745 Å, much shorter than in **9**. No hyperfine interactions were observed in the single-crystal spectrum.[26]

The paramagnetic susceptibility of **9**, calculated after a correction for diamagnetism estimated from tabulated Pascal's constants as -4.3×10^{-4} emu/mol, is quite similar to that of the Ni analogue (Figure 11). At room temperature the paramagnetic susceptibility is 3.6×10^{-4} emu/mol, and it decreases upon cooling to about 100 K, where it reaches a minimum. At lower temperatures the magnetic susceptibility becomes dominated by a Curie tail of impurities or defects and increases again. The EPR spectra suggest that these impurities are defects of undimerised $Pt(dcbdt)_2^-$ units. Taking into account the structure with dimers of paramagnetic $Pt(dcbdt)_2^-$ units, this behaviour can be described by a singlet-triplet model of antiferromagnetically coupled $S = 1/2$ dimers[27] and a low-temperature Curie tail, [Equation (1)], as previously done in the case of the Ni and Fe compounds.[9,12]

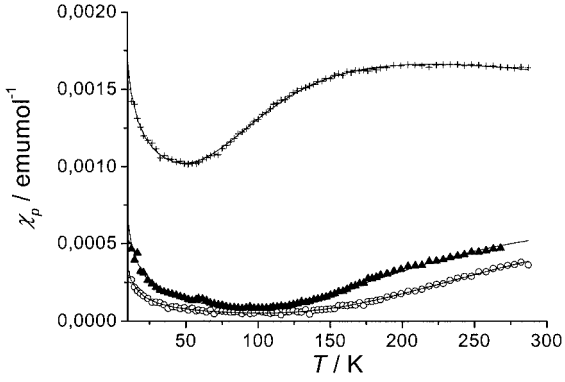

Figure 11. Magnetic susceptibility of $(n\mathrm{Bu_4N})[Pt(dcbdt)_2]$ (**9**) (circles), $(n\mathrm{Bu_4N})[Fe(dcbdt)_2]$ (squares)[12] and $(n\mathrm{Bu_4N})[Ni(dcbdt)_2]$ (triangles),[9] as a function of temperature; the line is a fit to Equation (1)

$$\chi_P = A + C/T + (Ng^2\mu_B^2/k_BT)[\exp(-2J/k_BT) + 3]^{-1} \quad (1)$$

A reasonable fit to Equation (1) was obtained with $J = 984$ K, $g = 2.9$, $A = 4 \times 10^{-5}$ emu/mol and a Curie tail corresponding to 1.5% of $S = 1/2$ spins. This g-value is certainly unrealistic because it is significantly larger than the highest g-value observed in the EPR spectra. This disagreement is probably due to the rather low temperature range of the experimental susceptibility data (when compared with the J value), which is inappropriate to obtain accurate fitting parameters.

Many Co^{III} bis(dithiolene) complexes are diamagnetic, but with some ligands, namely substituted benzodithiolates, high-spin $S = 1$ configurations are known.[13] The $[Co^{III}(dcbdt)_2]_2^{2-}$ compound (**5**) was found to be paramagnetic and its effective magnetic moment is also plotted in Figure 8 as a function of temperature. This paramagnetic behaviour demonstrates that the $[Co^{III}(dcbdt)_2]^-$ anions are in a high-spin $S = 1$ configuration. The effective magnetic moment observed is, however, significantly lower than the $S = 1$ value, demonstrating the presence of strong antiferromagnetic interactions. In spite of the crystal structure, with $[Co^{III}(dcbdt)_2]^-$ anions as dimers, packed side by side along a, the magnetisation data could not be fitted to any dimer or alternating-chain model.

Conclusion

In conclusion we have prepared and characterised several new members of the series of complexes $M(dcbdt)_2$ with different transition metals. These complexes are characterised by relatively low oxidation potentials, due to the extended nature of the ligands, and, as already described for M = Ni and Au, are expected to lead easily to partially oxidised, potentially electrically conducting. The Co^{II} complex is the first example of a pure Co compound in which hyperfine structure is observed in the solid state; the Co^{III} complex presents a high-spin configuration. The fuller use of these complexes in the preparation of conducting or magnetic molecular materials is presently under way.

Experimental Section

General: DMF, acetonitrile and dichloromethane were distilled from over phosphorus pentoxide and benzene was distilled from over sodium. Other chemicals were commercially obtained and

used without any further purification. 4,5-Dicyanobenzene-1,2-dithiol (**1**) was synthesised as described previously.[9] Elemental analyses were performed by the analytical services of IST and ITN. ^{1}H and ^{13}C NMR: Varian (300 MHz), [D$_6$]DMSO as solvent, and TMS as internal standard. IR: Perkin-Elmer 1330 spectrophotometer. VIS-UV-NIR: Cary 5G Varian spectrophotometer. Cyclic voltammetry data were obtained using a CV-50 W BAS Voltammetric Analyser. The measurements were performed at room temperature in acetonitrile solutions containing nBu$_4$ClO$_4$ as supporting electrolyte, with a scan rate of 100 mV/s, platinum working- and counter- electrodes and using a Ag/AgCl reference electrode.

EPR spectra in the range 4−300 K were obtained with an X-Band Bruker ESP 300E spectrometer equipped with a microwave bridge ER041XK, a rectangular cavity operating in T102 mode, a Bruker variable-temperature unit, an Oxford ESR-900 cryostat and a field controller ER 032M system. The modulation amplitude was kept well below the linewidth and the microwave power well below saturation.

Magnetic susceptibility measurements in the range 2−300 K were performed using a longitudinal Faraday system (Oxford Instruments) with a 7 T superconducting magnet, under a magnetic field of 5 T and forward- and reverse-field gradients of 1 T/m. Polycrystalline samples (10−15 mg) were placed inside a previously calibrated thin wall Teflon bucket. The force was measured with a microbalance (Sartorius S3D-V). Under these conditions the magnetisation was found to be proportional to the applied magnetic field.

Tetrabutylammonium Salt of Gold(III) Bis(4,5-dicyanobenzene-1,2-dithiolate) (nBu$_4$N)[Au(dcbdt)$_2$] (2): Compound **1** (0.2 g, 1.04 mmol) was dissolved in 5 mL of aqueous NaOH (5%). A solution of nBu$_4$NBr (0.17 g, 0.52 mmol) in EtOH/H$_2$O (1:1; 5 mL) was added, followed by a solution of KAuCl$_4$ (0.22 g, 0.52 mmol) in the same solvent. The mixture was stirred and a green precipitate was formed almost immediately. The solution was filtered and the precipitate was washed with EtOH. The crude material was recrystallised from acetone/iBuOH to give **2** as light-green needles (0.1 g, 1.2 mmol, 25%). M.p. 249−250 °C. ^{1}H NMR (300 MHz, [D$_2$]DCM, 25 °C, TMS): δ = 1.00 (t, J = 8.4 Hz, 12 H, CH$_3$), 1.41 (m, 8 H, CH$_2$), 1.59 (m, 8 H, CH$_2$), 3.07 (t, J = 7.2 Hz, 8 H, CH$_2$), 7.50 (s, 4 H, Ar−H) ppm. ^{13}C NMR (300 MHz, [D$_2$]DCM, 25 °C, TMS): δ = 13.77, 20.09, 24.26, 59.57, 113.77, 116.80, 132.98, 143.24) ppm. IR (KBr pellet): $\tilde{\nu}$ = 3060 (w, Ar−H), 2960−2860 (m, C−H), 2220 (s, C≡N), 1550 (w, C=C), 350 (w, S−Au) cm^{-1}. UV/Vis (CH$_2$Cl$_2$): λ_{max} (ε) = 264.2 (8500), 304.3 (34800), 367.6 (3300 mol^{-1} dm^3 cm^{-1}). C$_{32}$H$_{40}$AuN$_5$S$_4$ (820.02): calcd. C 46.87, H 4.93, N 8.54, S 15.64; found C 47.09, H 4.86, N 8.33, S 15.56.

Tetrabutylammonium Salt of Cobalt(II) Bis(4,5-dicyanobenzene-1,2-dithiolate) (nBu$_4$N)$_2$[Co(dcbdt)$_2$] (3): Compound **1** (0.48 g, 2.50 mmol) was dissolved in 5 mL of aqueous NaOH (5%). A solution of nBu$_4$NBr (0.80 g, 2.50 mmol) in EtOH/H$_2$O (1:1; 5 mL) was added, followed by a solution of CoCl$_2$·6H$_2$O (0.30 g, 1.26 mmol) in the same solvent. The mixture was stirred and a dark-blue precipitate was formed almost immediately. The solution was filtered and the precipitate was washed with EtOH. The crude material was recrystallised from acetone/iBuOH to give **3** as dark-blue crystals (0.64 g, 0.693 mmol, 55%). M.p. 254−255 C. IR (KBr pellet): $\tilde{\nu}$ = 3060 (w, Ar−H), 2960−2860 (m, C−H), 2220 (s, C≡N), 1550 (w, C=C), 530 (w, S−Co) cm^{-1}. UV/Vis (CH$_2$Cl$_2$): λ_{max} (ε) = 293.1 (91300), 322.0 (72600), 364.3 (41700), 589.0 (6700), 645.1 nm (17800 mol^{-1} dm^3 cm^{-1}). C$_{48}$H$_{76}$CoN$_6$S$_4$ (924.34): calcd. C 62.37, H 8.28, N 9.09, S 13.87; found C 61.10, H 8.13, N 9.42, S 14.94.

Tetrabutylammonium Salt of Cobalt(III) Bis(4,5-dicyanobenzene-1,2-dithiolate) (nBu$_4$N)[Co(dcbdt)$_2$] (4): A solution of I$_2$ (47.7 mg, 0.18 mmol) in acetone was added to a solution of **3** (0.17 g, 0.18 mmol) in acetone (50 mL). The solution was stirred until a colour change to dark green was observed. Ethanol was added and the solution was slowly evaporated to give **4** as dark-green needles (54.5 mg, 0.08 mmol, 46%). This compound can be also prepared directly from the ligand and CoCl$_2$ in the presence of air as follows: Compound **1** (0.17 g, 0.89 mmol) was dissolved in 5 mL of aqueous NaOH (5%). A solution of nBu$_4$NBr (0.14 g, 0.44 mmol) in EtOH/H$_2$O (1:1) (5 mL) was added, followed by a solution of CoCl$_2$·6H$_2$O (0.11 g, 0.44 mmol) in the same solvent. The mixture was stirred for 2 hours while a dark green precipitate was formed. The solution was filtered and the precipitate was washed with EtOH. The crude material was recrystallised from EtOH to give **4** as black/green crystals (77.3 mg, 0.11 mmol, 26%). M.p. 288−289 °C. ^{1}H NMR (300 MHz, [D$_6$]DMSO, TMS): δ = 0.90 (s, 12 H, CH$_3$), 1.27 (m, 8 H, CH$_2$), 1.49 (m, 8 H, CH$_2$), 3.08 (s, 8 H, CH$_2$) ppm. ^{13}C NMR (300 MHz, [D$_6$]DMSO, TMS): δ = 18.52, 24.21, 28.03, 62.50) ppm. IR (KBr pellet): $\tilde{\nu}$ = 3060 (w, Ar−H), 2980−2880 (m, C−H), 2220 (s, C≡N), 1560 (w, C=C), 430 (w, S−Co) cm^{-1}. UV/Vis (CH$_2$Cl$_2$): λ (ε) = 285.3 nm (8100 mol^{-1} dm^3 cm^{-1}), 318.0 (7000), 364.0 (4300), 411.9 (2100), 645.0 (1500). C$_{32}$H$_{40}$CoN$_5$S$_4$ (681.87): calcd. C 56.35, H 5.93, N 10.28, S 18.83; found C 57.23, H 6.22, N 10.25, S 18.84.

Tetrabutylammonium Salt of Copper(II) Bis(4,5-dicyanobenzene-1,2-dithiolate) (nBu$_4$N)$_2$[Cu(dcbdt)$_2$] (5): Compound **1** (0.30 g, 1.56 mmol) was dissolved in 5 mL of aqueous NaOH (5%). A solution of nBu$_4$NBr (0.51 g, 1.56 mmol) in EtOH/H$_2$O (1:1; 5 mL) was added, followed by a solution of CuCl$_2$·2H$_2$O (0.13 g, 0.78 mmol) in the same solvent. The mixture was stirred and a brown precipitate was formed almost immediately. The solution was filtered and the precipitate was washed with EtOH. The crude material was recrystallised from acetone to give **5** as brown needles (0.19 g, 0.20 mmol, 26%). M.p. 243−245 °C. ^{1}H NMR (300 MHz, [D$_6$]DMSO, 25 °C, TMS): δ = 0.99 (s, 24 H, CH$_3$), 1.48 (m, 16 H, CH$_2$), 1.86 (m, 16 H, CH$_2$), 3.59 (m, 16 H, CH$_2$) ppm. ^{13}C NMR (300 MHz, [D$_6$]DMSO, 25 °C, TMS): δ = 15.32, 20.55, 24.55, 50.49 ppm. IR (KBr pellet): $\tilde{\nu}$ = 3060 (w, Ar−H), 2960−2860 (m, C−H), 2220 (s, C≡N), 1540 (w, C=C), 430 (w, S−Cu) cm^{-1}. UV/Vis (CH$_2$Cl$_2$): λ (ε) = 320.1 nm (72500 mol^{-1} dm^3 cm^{-1}), 386.5 (18800). C$_{48}$H$_{76}$CuN$_6$S$_4$ (928.95): calcd. C 62.05, H 8.26, N 9.05, S 13.81; found C 61.74, H 7.98, N 8.90, S 14.13.

Tetrabutylammonium Salt of Copper(III) Bis(4,5-dicyanobenzene-1,2-dithiolate) (nBu$_4$N)[Cu(dcbdt)$_2$] (6): A solution of I$_2$ (51.9 mg, 0.20 mmol) in acetone was added to a solution of **5** (0.17 g, 0.18 mmol) in acetone (50 mL). The solution was stirred until a colour change to green was observed. Ethanol was added and the solution was slowly evaporated to give **6** as dark-green needles (90.2 mg, 0.13 mmol, 64%). M.p. 233−234 °C. ^{1}H NMR (300 MHz, [D$_6$]acetone, 25 °C, TMS): δ = 0.98 (t, J = 7.2 Hz, 12 H, CH$_3$), 1.44 (m, 8 H, CH$_2$), 1.84 (m, 8 H, CH$_2$), 3.45 (t, J = 8.6 Hz, 8 H, CH$_2$), 7.51 (s, 4 H, Ar−H) ppm. ^{13}C NMR (300 MHz, [D$_6$]acetone, 25 °C, TMS): δ = 13.91, 20.41, 24.44, 59.39, 114.22, 126.73, 131.33, 143.73 ppm. IR (KBr pellet): $\tilde{\nu}$ = 3060 (w, Ar−H), 2980−2880 (m, C−H), 2220 (s, C≡N), 1510 (s, C=C), 420 (w, S−Cu) cm^{-1}. UV/Vis (CH$_2$Cl$_2$): λ (ε) = 300.1 nm (137600), 395.0 (58200 mol^{-1} dm^3 cm^{-1}). C$_{32}$H$_{40}$CuN$_5$S$_4$ (686.49): calcd. C 55.99, H 5.87, N 10.20, S 18.68; found C 55.03, H 6.47, N 9.91, S 19.19.

Tetrabutylammonium Salt of Palladium(II) Bis(4,5-dicyanobenzene-1,2-dithiolate) (nBu$_4$N)$_2$[Pd(dcbdt)$_2$] (7): Compound **1** (0.41 g, 2.13 mmol) was dissolved in 5 mL of aqueous NaOH (5%). A solu-

tion of nBu$_4$NBr (0.70 g, 2.17 mmol) in EtOH/H$_2$O (1:1; 5 mL) was added, followed by a solution of K_2PdCl_4 (0.33 g, 1.01 mmol) in the same solvent. The mixture was stirred and an orange precipitate was formed almost immediately. The solution was filtered and the precipitate was washed with EtOH. The crude material was recrystallised from acetone/iBuOH to give **7** as red crystals (0.62 g, 0.64 mmol, 63%). M.p. 263−264 °C. ^{1}H NMR (300 MHz, [D$_6$]DMSO, 25 °C, TMS): δ = 0.93 (t, J = 7.2 Hz, 24 H, CH$_3$), 1.31 (m, 16 H, CH$_2$), 1.56 (m, 16 H, CH$_2$), 3.32 (t, J = 6.0 Hz, 16 H, CH$_2$), 7.28 (s, 4 H, Ar−H) ppm. ^{13}C NMR (300 MHz, [D$_6$]DMSO, 25 °C, TMS): δ = 14.17, 19.88, 23.74, 58.24, 96.41, 116.02, 131.49 ppm. IR (KBr pellet): ν̃ = 3060 (w, Ar−H), 2980−2840 (m, C−H), 2200 (s, C≡N), 1530 (m, C=C), 430 (w, S−Pd) cm^{-1}. UV/Vis (CH$_2$Cl$_2$): λ_{max} (ε) = 300.7 nm (53800), 345.0 (72300), 425.2 (13800 mol^{-1} dm^3 cm^{-1}). $C_{48}H_{76}N_6PdS_4$ (971.81): calcd. C 59.32, H 7.88, N 8.64, S 13.20; found C 58.51, H 8.11, N 8.86, S 13.05.

Tetrabutylammonium Salt of Platinum(II) Bis(4,5-dicyanobenzene-1,2-dithiolate) (nBu$_4$N)$_2$[Pt(dcbdt)$_2$] (8): Compound **1** (0.28 g, 1.46 mmol) was dissolved in 5 mL of aqueous NaOH (5%). A solution of nBu$_4$NBr (0.47 g, 1.46 mmol) in EtOH/H$_2$O (1:1; 5 mL) was added, followed by a solution of K_2PtCl_4 (0.52 g, 1.25 mmol) in the same solvent. The mixture was stirred and a red precipitate was formed almost immediately. The solution was filtered and the precipitate was washed with EtOH. The crude material was recrystallised from acetone/iBuOH to give **8** as red crystals (0.38 g, 0.36 mmol, 35%). M.p. 270−271 °C. ^{1}H NMR (300 MHz, [D$_2$]DCM, 25 °C, TMS): δ = 0.92 (t, J = 5.3 Hz, 24 H, CH$_3$), 1.28 (m, 16 H, CH$_2$), 1.53 (m, 16 H, CH$_2$), 3.15 (s, 16 H, CH$_2$), 7.36 (s, 4 H, Ar−H) ppm. ^{13}C NMR (300 MHz, [D$_2$]DCM, 25 °C, TMS): δ = 12.13, 17.85, 21.73, 56.17, 96.74, 111.48, 130.20, 143.11 ppm. IR (KBr pellet): ν̃ = 3060 (w, Ar−H), 2960−2860 (m, C−H), 2210 (s, C≡N), 1525 (m, C=C), 530 (m, S−Pt) cm^{-1}. UV/Vis (CH$_2$Cl$_2$): λ_{max} (ε) = 230.4 nm (42400), 279.0 (38300), 382.3 (31900), 449.8 (7800 mol^{-1} dm^3 cm^{-1}). $C_{48}H_{76}N_6PtS_4$ (1060.50): calcd. C 54.36, H 7.22, N 7.92, S 12.09; found C 55.73, H 7.61, N 8.12, S 12.74.

Tetrabutylammonium Salt of Platinum(III) Bis(4,5-dicyanobenzene-1,2-dithiolate) (nBu$_4$N)[Pt(dcbdt)$_2$] (9): A solution of I$_2$ (45.0 mg, 0.18 mmol) in acetone was added to a solution of **8** (0.38 g, 0.36 mmol) in acetone (100 mL). The solution was stirred until a colour change to green was observed. Ethanol was added and the solution was slowly evaporated to give **9** as dark-green needles (99.0 mg, 0.12 mmol, 33%). M.p. 250−251 °C. ^{1}H NMR (300 MHz, [D$_2$]DCM, 25 °C, TMS): δ = 0.94 (t, J = 7.1 Hz, 12 H, CH$_3$), 1.32 (m, 8 H, CH$_2$), 1.58 (m, 8 H, CH$_2$), 3.18 (s, 8 H, CH$_2$) ppm. ^{13}C NMR (300 MHz, [D$_2$]DCM, 25 °C, TMS): δ = 13.39, 18.89, 23.54, 53.79 ppm. IR (KBr pellet): ν̃ = 3060 (w, Ar−H), 2960−2860 (m, C−H), 2220 (s, C≡N), 1550 (w, C=C), 420 (w, S−Pt) cm^{-1}. UV/Vis (CH$_2$Cl$_2$): λ_{max} (ε) = 280.2 (80600), 347.1 nm (20400 mol^{-1} dm^3 cm^{-1}). $C_{32}H_{40}N_5PtS_4$ (818.03): calcd. C 46.98, H 4.94, N 8.56, S 15.68; found C 48.40, H 4.91, N 8.48, S 15.14.

Tetrabutylammonium Salt of Zinc(II) Bis(4,5-dicyanobenzene-1,2-dithiolate) (nBu$_4$N)$_2$[Zn(dcbdt)$_2$] (10): Compound **1** (0.14 g, 0.73 mmol) was dissolved in 5 mL of aqueous NaOH (10%). A solution of nBu$_4$NI (0.26 g, 0.73 mmol) in EtOH/H$_2$O (1:1; 5 mL) was added, followed by a solution of $ZnCl_2$ (0.05 g, 0.36 mmol) in the same solvent. The mixture was stirred and an orange precipitate was formed almost immediately. The solution was filtered and the precipitate was washed with EtOH. The crude material was recrystallised from acetonitrile/iBuOH to give **10** as orange crystals (0.22 g, 0.24 mmol, 65%). M.p. 205−206 °C. ^{1}H NMR (300 MHz, [D$_6$]acetone, 25 °C, TMS): δ = 0.96 (t, J = 7.4 Hz, 24 H, CH$_3$), 1.41 (m, 16 H, CH$_2$), 1.76 (m, 16 H, CH$_2$), 3.39 (m, 16 H, CH$_2$), 7.69 (s, 4 H, Ar−H) ppm. ^{13}C NMR (300 MHz, [D$_6$]acetone, 25 °C TMS): δ = 13.83, 20.31, 24.43, 59.36, 104.15, 114.02, 118.46, 132.88 ppm. IR (KBr pellet): ν̃ = 3040−3090 (w, Ar−H), 2960−2860 (m, C−H), 2240 (s, C≡N), 1540 (s, C=C), 420 (w, S−Zn) cm^{-1}. UV/Vis (CH$_2$Cl$_2$): λ_{max} (ε) = 310.3 (43400), 385.5 nm (20500 mol^{-1} dm^3 cm^{-1}). $C_{48}H_{76}N_6S_4Zn$ (930.79): calcd. C 61.94, H 8.23, N 9.03, S 13.78; found C 61.87, H 8.92, N 2.3, S 13.78.

X-ray Crystallographic Study: All diffraction measurements were made at room temperature with the crystals mounted in a glass capillary. An Enraf−Nonius TURBO CAD4 diffractometer equipped with graphite monochromated Cu-K_α radiation (λ = 1.5418 Å) was used for measurements of compounds **3** and **6**. All the other crystals were measured on an Enraf−Nonius CAD4 diffractometer using graphite-monochromated Mo-K_α radiation (λ = 0.71069 Å) in the ω-2θ scan mode. Lorentz, polarisation effects and empirical absorption correction based on psi-scan were applied to the collected intensities. The structures were solved by direct methods using SIR97[28] and refined by full-matrix least-squares methods using the program SHELXL-97[29] and the winGX software package.[30] All non-hydrogen atoms were refined anisotropically. Hydrogen atoms were placed in calculated positions. In the compound (nBu$_4$N)[Cu(dcbdt)$_2$] (**6**) the cation unit was found to be disordered and was refined over two positions with occupancy factors of 0.608 and 0.392, respectively. The cation disorder of compounds **2** and **9** could not be fitted by any model. Molecular graphics were prepared with ORTEP3[31] and SCHAKAL-97.[32] Crystal data and structure refinement details are summarised in Table 1 and Table 2.

CCDC-213103, -213104, -213105, -213106, -213107, -213108, -213109 and -213110 for compounds **2**, **4**, **6**, **9**, **3**, **7**, **8** and **10**, respectively, contain the supplementary crystallographic data for this paper. These data can be obtained free of charge at www.ccdc.cam.ac.uk/conts/retrieving.html [or from the Cambridge Crystallographic Data Centre, 12, Union Road, Cambridge CB2 1EZ, UK; Fax: (internat.) +44-1223/336-033; E-mail: deposit@ccdc.cam.ac.uk].

Acknowledgments

This work was partially supported by FCT (Portugal) under contract POCTI 35452/99. HA also acknowledges FCT for the doctoral grant. This work also benefited from COST action D14/0003/99.

[1] N. Robertson, L. Cronin, *Coord. Chem. Rev.* **2002**, *227*, 93−127.
[2] L. Alcácer, H. Novais, in: *Extended Linear Chain Compounds* (Ed.: J. S. Miller), Plenum Press, New York, **1983**, vol. 3, pp. 319−351.
[3] P. Cassoux, L. Valade, H. Kobayashi, A. Kobayashi, R. A. Clark, A. E. Underhill, *Coord. Chem. Rev.* **1991**, *110*, 115−160.
[4] P. I. Clemenson, *Coord. Chem. Rev.* **1990**, *106*, 171−203.
[5] D. Coucouvanis, *Prog. Inorg. Chem.* **1970**, *11*, 233−371.
[6] J. A. McCleverty, *Prog. Inorg. Chem.* **1968**, *10*, 49.
[7] V. Gama, R. T. Henriques, M. Almeida, L. Veiros, M. J. Calhorda, A. Meetsma, J. L. De Boer, *Inorg. Chem.* **1993**, *32*, 3705−3711.
[8] V. Gama, R. T. Henriques, G. Bonfait, M. Almeida, A. Meetsma, S. V. Smaalen, J. L. De Boer, *J. Am. Chem. Soc.* **1992**, *114*, 1986−1989.
[9] D. Simão, H. Alves, D. Belo, S. Rabaça, E. B. Lopes, I. C. Santos, V. Gama, M. T. Duarte, R. T. Henriques, H. Novais, M. Almeida, *Eur. J. Inorg. Chem.* **2001**, 3119−3126.

[10] H. Alves, D. Simão, E. B. Lopes, D. Belo, V. Gama, M. T. Duarte, H. Novais, R. T. Henriques, M. Almeida, *Synth. Met.* **2001**, *120*, 1011−1012.
[11] H. Alves, I. C. Santos, E. B. Lopes, D. Belo, V. Gama, D. Simão, H. Novais, M. T. Duarte, R. T. Henriques, M. Almeida, *Synth. Met.* **2003**, *133−134*, 397−399.
[12] H. Alves, D. Simão, H. Novais, I. C. Santos, C. Giménez-Saiz, V. Gama, J. C. Waerenborgh, R. T. Henriques, M. Almeida, *Polyhedron* **2003**, *22*, 2481−2486.
[13] M. J. Baker−Hawkes, E. Billig, H. B. Grey, *J. Am. Chem. Soc.* **1966**, *88*, 4870−4875.
[14] H. Alves, E. B. Lopes, I. C. Santos, R. T. Henriques, M. Almeida, paper to be published.
[15] G. R. Lewis, I. Dance, *J. Chem. Soc., Dalton Trans.* **2000**, 3176.
[16] N. M. Comerlato, W. T. A. Harrison, R. A. Howie, J. N. Low, A. C. Silvino, J. L. Wardell, S. M. S. V. Wardell, *Acta Crystallogr., Sect. C* **2002**, *58*, 105.
[17] J. Stach, R. Kirmse, J. Sieler, U. Abram, W. Dietzsch, R. Bottcher, L. K. Hansen, H. Vergooossen, M. C. M. Gribnau, C. P. Keijzers, *Inorg. Chem.* **1986**, *25*, 1369.
[18] W. C. Hamilton, I. Bernal, *Inorg. Chem.* **1967**, *6*, 2003.
[19] A. L. Balch, I. G. Dance, R. H. Holm, *J. Am. Chem. Soc.* **1968**, *90*, 1139.
[20] J. V. Rodrigues, I. C. Santos, V. Gama, R. T. Henriques, J. C. Waerenborgh, M. T. Duarte, M. Almeida, *J. Chem. Soc., Dalton Trans.* **1994**, 2655−2660.
[21] J. A. Weil, J. R. Bolton, J. Wertz, *Electron Paramagnetic Resonance*, Wiley-Interscience Publication, New York, **1994**.
[22] F. A. Walker, J. Bowen, *J. Am. Chem. Soc.* **1985**, *107*, 7632−7635.
[23] B. M. Hoffman, D. L. Diemente, F. Basolo, *J. Am. Chem. Soc.* **1970**, *92*, 61−65.
[24] R. Kirmse, W. Dietzsch, B. V. Solovev, *J. Inorg. Nucl. Chem.* **1977**, *39*, 1157−1160.
[25] I. Kochurani, H. B. Singh, J. P. Jasinski, E. S. Paight, R. J. Butcher, *Polyhedron* **1997**, *16*, 3505−3510.
[26] J. K. Barton, D. J. Szalda, H. N. Rabinowitz, J. V. Waszczak, S. J. Lippard, *J. Am. Chem. Soc.* **1979**, *101*, 1434−1441.
[27] R. L. Carlin, *Magnetochemistry*, Springer-Verlag, Berlin, **1986**.
[28] A. Altomare, M. C. Burla, M. Camalli, G. Cascarano, G. Giacovazzo, A. Guagliardi, A. G. G. Moliterni, G. Polidori, R. Spagna, *J. Appl. Crystallogr.* **1999**, *32*, 115−119.
[29] G. M. Sheldrick, *SHELXL-97, A Program for Crystal Structure Refinement*, University of Göttingen, Göttingen, **1997**.
[30] L. J. Farrugia, *J. Appl. Crystallogr.* **1999**, *32*, 837−838.
[31] L. J. Farrugia, *J. Appl. Crystallogr.* **1997**, *30*, 565.
[32] E. Keller, *SCHAKAL-97, A Computer Program for the Representation of Molecular and Crystallographic Models*, Kristallographisches Institut der Universität Freiburg i. Br., Germany, Freiburg, **1997**.

Received July 18, 2003
Early View Article
Published Online February 10, 2004

